Int. J. Electrochem. Sci., 15 **(2020)** 26 – 38, doi: 10.20964/2020.01.20

International Journal of
ELECTROCHEMICAL
SCIENCE
www.electrochemsci.org

Corrosion Assessment of Sn–Ni Alloy Coatings using Neutral Salt Spray Tests and Electrochemical Methods

Chuanyun Wan[*], *Li Zhang, Xiya Liu*

School of Chemical and Environmental Engineering, Shanghai Institute of Technology, Shanghai 201418
[*]E-mail: cywan@sit.edu.cn

Received: 3 September 2019 / *Accepted:* 24 October 2019 / *Published:* 30 November 2019

To elucidate the excellent anti-corrosion properties of a Sn-Ni alloy compared to those of a pure Sn coating, the accelerated corrosion behavior of an as-deposited Sn-Ni alloy coating from a pyrophosphate bath was investigated by salt spray tests and electrochemical methods in a neutral mist of 5% NaCl solution. Scanning electron microscopy (SEM), X-ray photoelectron spectroscopy (XPS), X-ray diffraction (XRD), potentiodynamic and electrochemical impedance spectroscopy (EIS) techniques were used to study the changes in the physical and electrochemical properties of the Sn-Ni alloy coating during salt spray testing. A thin compact passive film consisting of metal oxides (Sn and Ni) formed on the surface of the as-deposited Sn-Ni alloy coating, resulting in an improved corrosion resistance in the neutral mist compared to that of a pure Sn coating. The initial passive film was destroyed, and the metallic metals (Sn and Ni) were dissolved and formed oxides during the initial stage of salt spray testing. The composition of the oxide film on the surface of Sn-Ni alloy varied with the duration of the salt spraying. Finally, a compact passive film consisting of $Ni(OH)_2$, SnO and SnO_2 was produced and remained stable in the neutral solution when the salt spray testing time reached 72 h. The regeneration of a compact passive film on the surface of Sn-Ni alloy demonstrated excellent resistance to electrochemical corrosion of the Sn-Ni alloy in the neutral chloride-containing solution. The good corrosion resistance of the Sn–Ni alloy supports the application of Sn-Ni alloys in neutral solutions.

Keyword: Sn–Ni Alloy; Salt Spray Test; Corrosion Resistance

1. INTRODUCTION

Sn-Ni alloys have been of great interest in industrial applications because they have a significant resistance to corrosion, wear, tarnishing and also have a high hardness [1]. Hence, detailed investigations of Sn-Ni alloys are ongoing. In the early years of the 20th century, Sn–Ni alloys, one of the key systems for lead-free soldering, have been intensively investigated as an interlayer between copper and gold deposits to increase their wear resistance and as a resist material for the etching

process that is used for printed circuit board manufacturing in electronic applications [2-6]. Later, the development of electroplating technology for Sn-Ni alloys widened its application field. For example, electrodeposited chromium has been applied to different industrial products, such as automobiles, due to its high hardness, wear and corrosion resistance [7]. However, the chromium (VI) electroplating process usually produces air pollution and water contamination [8, 9]. In light of the health and environmental issues, Sn-Ni alloy plating is a good substitute for chromium plating because of its high corrosion resistance and high resistance to tarnishing [10, 11]. Sn has been found to be a promising anode material for lithium-ion batteries [12-14], and Sn-Ni alloys also show application potential as an anode material in lithium-ion batteries [15-17] and pseudocapacitors [18] or as cathodes for hydrogen evolution in alkaline solutions [19].

As an electrodeposited coating, the corrosion resistance of Sn-Ni alloy is the reason for its decorative and engineering applications. Many works have focused on how to deposit Sn-Ni alloys [20-23] and found that the corrosion stability of Sn–Ni alloys is due to the presence of a stable "natural" oxide film on the alloy surface that forms upon air exposure [24, 25]. However, the anti-corrosion mechanism of the oxide film has not been reported. Several corrosion studies on Sn-Ni alloys have been reported, and electrochemical techniques (cyclic voltammetry, polarization curves and ambient continuous immersion in aerated solution) have been applied to investigate the corrosion and passivation behaviors of Sn-Ni alloys [24-28]. However, few studies have been reported that elucidate the corrosion behaviors of Sn-Ni alloys [26, 28]. The salt spray test is an effective technique to study the corrosion resistance of materials and surface coatings in an accelerating mode [29, 30]. Studying the composition of the Sn-Ni surface during salt spraying is a good way to understand the action of the oxide film that covers the surface in a corrosive environment and can further elucidate the excellent anti-corrosion behavior of Sn-Ni compared with that of pure Sn coatings. In this study, Sn-Ni alloy coatings were deposited on copper in a pyrophosphate bath. The corrosion behaviors of the coatings were tested by the neutral salt spray method, and the corresponding corrosion mechanism was investigated.

2. EXPERIMENTAL

Electrodeposition of the Sn–Ni alloy coating was carried out in a pyrophosphate bath containing 230 g L^{-1} $K_4P_2O_7 \cdot 3H_2O$, 45 g L^{-1} $NiSO_4 \cdot 6H_2O$, 30 g L^{-1} $SnCl_2 \cdot 2H_2O$, 12 g L^{-1} NH_4Cl, and 2 g L^{-1} saccharin sodium. Solutions were freshly prepared from analytical reagents and distilled water. The pH of the solutions was adjusted and controlled to a value of 8.5 using ammonia, and the temperature was maintained at 45 °C using a constant-temperature bath. The current density of metal deposition was 1A dm^{-2}. Pure copper was used as the substrate. Before metal deposition, Cu was mechanically polished with 2000-mesh sandpaper, cleaned ultrasonically in distilled water for 10 min, activated in 5% H_2SO_4 for 30 s, and finally washed with distilled water. For comparison, a pure Sn coating was also electrodeposited in a pyrophosphate bath that did not contain nickel salt. The thickness of all samples for testing was controlled to be in the range of 5±0.5 μm.

The Sn-Ni alloy and pure Sn samples were exposed to a continuous indirect spray of 5 wt. % neutral NaCl solution in a salt spray chamber at 35 °C designed for salt spray tests. When testing, the weighted samples were placed facing upwards on the bracket and tilted at 30 degrees to prevent effusion. The different exposure times were applied, and the salt spray test time was up to 120 h, at which apparent corrosion was visible on the surface of the pure Sn coating. After exposure, the samples were first gently washed in clean and running distilled water to remove salt deposits and then washed with absolute ethanol. Finally, the washed samples were dried with nitrogen gas.

The electrochemical tests of the samples were conducted in a neutral 5 wt. % NaCl solution using a three-electrode cell. The samples with the different salt spray testing times were used as the working electrode, while a platinum sheet and a calomel electrode (SCE) acted as the counter electrode and the reference electrode, respectively. The potentiodynamic corrosion curves were carried out at a potential sweep rate of 1 mV s^{-1}. The electrochemical impedance spectroscopy (EIS) experiments were measured from 0.1 Hz to 100 KHz at the open circuit potential (OCP) with an alternate current amplitude of 5 mV. All the electrochemical experiments were carried out on a Gamry Reference 600+ electrochemical working station.

The crystallographic phases on the surface of the samples were identified with X-ray diffraction (XRD; PANalytical X'pert Pro, Almeo, The Netherlands) with CuKα radiation at a λ=1.54187 Å and voltage of 30KV. The morphologies of the coatings were examined using scanning electron microscopy (SEM; FEI Nova NanoSEM x30) equipped with energy dispersive X-ray spectroscopy (EDS). The chemical composition of the Sn-Ni alloys was determined by EDS analysis (measurement area was 1 μm×1 μm) and the reported results were the average of three measurements. X-ray photoelectron spectroscopy (XPS; Thermo Scientific ESCALAB 250Xi spectrometer) was also carried out to analyze the chemical state of the coating in the salt spray test.

3. RESULTS AND DISCUSSION

3.1 Characterization of Sn-Ni alloy

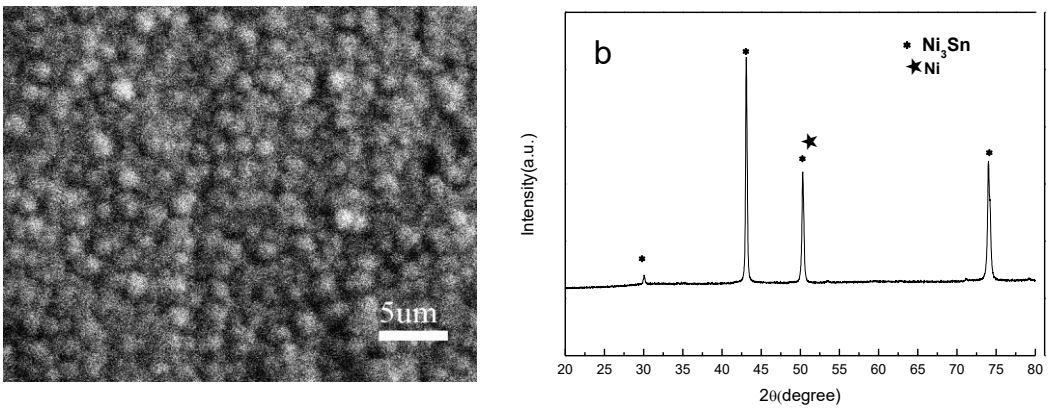

Figure 1. SEM image (a) and XRD patterns (b) of the as-deposited Sn-Ni alloy coating

The morphology of the Sn-Ni alloy coating obtained from the pyrophosphate bath is presented in Fig. 1a. The Sn-Ni alloy deposit is compact and consists of fine grains. EDS analysis was performed to determine the composition of the obtained Sn-Ni alloy, and it was found that the weight percent of Sn in the Sn-Ni alloy is (67±2)% and that of Ni is (33±2)%. The XRD patterns of the as-deposited Sn-Ni alloy coating are presented in Fig. 1b. It is clearly shown that there are three strong peaks at 43.4°, 50.6° and 74.2° and a weak peak at 30°. According to the XRD standard diffraction pattern from the Joint Committee on Powder Diffraction Standard (JCPDS), the three strong peaks can be assigned to the Ni_4Sn phase (JCPDS 10-0193). However, some works based on the theoretical assessment (CALPHAD method) of the Ni-Sn system exclude the existence of this phase [3, 31, 32]. According to Schmetterer et al. [3], a sample with nominal composition of $Ni_{80}Sn_{20}$ consists of two phases: Ni and Ni_3Sn. All the peaks shown in Fig. 1b can be assigned to the Ni-rich Ni_3Sn phase, and the peak at approximately 50.6° is the result of an overlap of the Ni and Ni_3Sn peaks [3]. Here, we concluded that the phase of the obtained Sn-Ni alloy is a Ni-rich Ni_3Sn phase.

3.2 Corrosion behavior of the Sn-Ni alloy in salt spray test

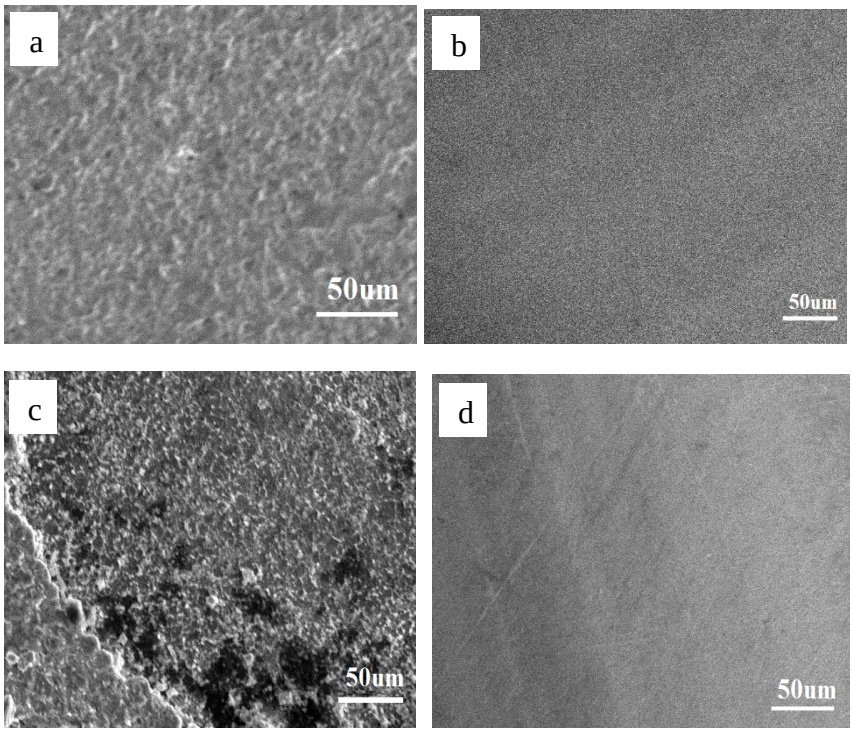

Figure 2. Macro morphologies of coatings before (a Sn; b Sn-Ni) and after salt spray test (c: Sn-120h, d: Sn-Ni-120h)

The Sn-Ni alloy coatings and pure Sn coatings were both treated in salt spray mode for subsequent corrosion measurement. Fig. 2 presents the macromorphologies of the tested coatings before and after salt spray testing for 120 h. Prior to the salt spray test, the morphologies of the Sn-Ni alloy coating and pure Sn coating are fairly homogeneous and uniform. Both coatings appear bright. After salt spray testing, severe corrosion occurs for the pure Sn coating, and corrosion pits are visible

on its surface. No obvious corrosion pits are detected on the surface of the Sn-Ni alloy coating, but it was slightly tarnished. Compared with that of the pure Sn metal coating, the enhanced corrosion resistance of the Sn-Ni alloy coating is clearly verified by the salt spray test.

Fig. 3 shows the weight loss of the Sn-Ni alloy coating and pure Sn coating at different salt spray testing times. It is clear that high corrosion rates occur during the first 24 h of salt exposure for both the Sn-Ni alloy coating and pure Sn coating. After 24 h of testing, the weight loss of the pure Sn coating is much larger than that of the Sn-Ni alloy coating, indicating that the Ni-doped Sn alloy coating has an improved corrosion resistance compared to that of the pure Sn coating.

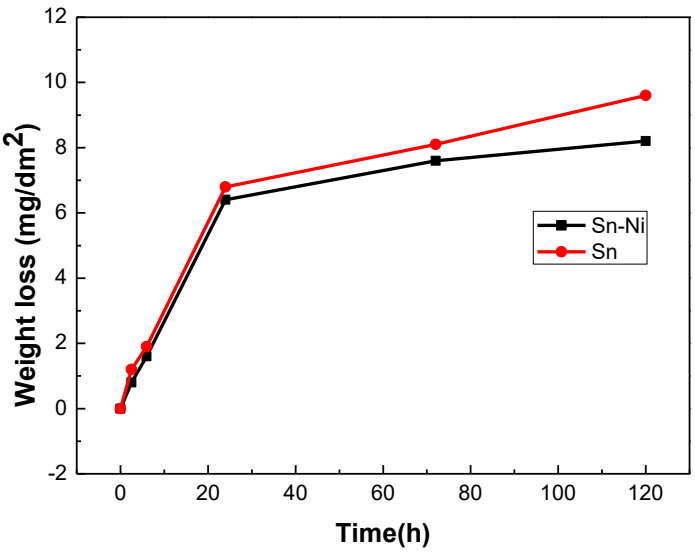

Figure 3. Weight loss of Sn-Ni alloy coating and pure Sn coating at different salt spray testing times

3.3 Characterization of the corrosion behavior

The Sn-Ni alloy exhibits an improved corrosion resistance compared to that of the pure Sn coating. To elucidate the anti-corrosion behavior of the Sn-Ni alloy, Sn-Ni alloy samples that experienced different salt spraying times were collected and investigated with physical and electrochemical methods. XPS is an effective and powerful tool for determining elemental components and their chemical state. The surface corrosion of the Sn-Ni alloy can be easily obtained with XPS. The Ni $2p_{3/2}$ and Sn $Sn3d_{5/2}$ XPS spectra from the Sn-Ni alloy coatings exposed to the salt spray for different times are shown in Fig. 4a and b, respectively. For the as-deposited Sn-Ni alloy coating, the Ni $2p_{3/2}$ peaks located at 852.3 eV, 855.9 eV and 860.3 eV could be attributed to the binding energies of metallic Ni, $Ni(OH)_2$ and NiO[33, 34], respectively. The $Sn3d_{5/2}$ spectra show that there are three kinds of bonding energy for the Sn species on the surface of the Sn-Ni alloy coating. The main $Sn3d_{5/2}$ peak detected at 486.3 eV can be attributed to SnO, and the peaks found at 484.2 eV and 484.8±0.3 eV can be attributed to metallic tin [33, 35]. Evidently, there is an oxide film on the surface of the as-deposited Sn-Ni alloy coating. The oxide film consists of NiO, $Ni(OH)_2$, and SnO and is formed by

natural air. This oxide film, also called a passive film, should be responsible for the high corrosion resistance of the Sn-Ni alloy coatings [24, 25]. When a Sn-Ni alloy coating is exposed to salt spray, the composition of the oxide film covering the surface of the Sn-Ni alloy coating varies with the salt spray testing time. The contents of metallic Sn and Ni increase during the first 2.5 h of salt spraying, indicating that the oxide film is attacked and dissolved. The metallic species decrease with a further increase in the salt spray testing time, and there is no metallic Sn or Ni on the surface of the Sn-Ni alloy coating when the salt spraying time is up to 72 h, indicating that metallic Ni and Sn are gradually oxidized during the salt spraying test. Finally, the surface of the Sn-Ni alloy coating is completely covered by an oxide film composed of $Ni(OH)_2$, SnO and SnO_2 (bonding energies from 486.5-486.8 eV in the $Sn3d_{5/2}$ XPS spectrum). There is no evident change in the phase structure after 72 h of salt spray testing. The percentage of each phase under different testing times can be determined by $A(x)/A_{total}$, where A(x) is the area under the corresponding peak and A_{total} is the total area of the $Ni2p_{3/2}$ and $Sn3d_{5/2}$ peaks in the XPS curve. The proportion of each phase after peak-fitting and the Sn/Ni atomic ratios are both shown in Table 1. It can be observed that the composition of the Sn-Ni alloy surface varies with the salt spray testing time, indicating that Ni and Sn species dissolve due to the dissolved oxygen in the NaCl solution [24]. The following reactions may occur [36, 37]:

$$Ni+H_2O(aq.) \longrightarrow NiOH(ads.)^+ + 2e \quad (1)$$

$$NiOH^+ \longrightarrow NiO + H^+ \quad (2)$$

The metallic Sn is dissolved to form $Sn(OH)_2$ and $Sn(OH)_2$ and can be further oxidized to form $Sn(OH)_4$. $Sn(OH)_2$ and $Sn(OH)_4$ can both be dehydrated to produce thermodynamically stable tin oxides (SnO and SnO_2) [28, 38]; the reaction equations are as follows:

$$Sn + H_2O(aq.) \longrightarrow Sn(OH)_2 + 2H^+ + 2e \quad (3)$$

$$Sn(OH)_2 + H_2O(aq.) \longrightarrow Sn(OH)_4 + 2H^+ + 2e \quad (4)$$

$$Sn(OH)_2 \longrightarrow SnO + H_2O \quad (5)$$

$$Sn(OH)_4 \longrightarrow SnO_2 + H_2O \quad (6)$$

Due to the dissolution of the metallic species (Sn and Ni) and the transpassive dissolution of the metal oxides between the interface of the oxide film and the solution, the composition of the passive films formed on the surface of the Sn-Ni alloy coatings changes over the duration of the salt spraying during the initial stage of salt spray testing. After 72 h of salt spray testing, the surface of the Sn-Ni alloy coating is completely covered by a passive film composed of $Ni(OH)_2$, SnO and SnO_2. The “surface” atomic Sn/Ni ratio also changes greatly during the first 24 h of testing. Before salt spray testing, the Sn/Ni atomic ratio on the surface of Sn-Ni alloy coating is 2.7 and decreases to ca. 1.2 after 24 h the testing and finally maintains this value with an increase in the testing time. A decrease in the Sn/Ni atomic ratio may be due to the rapid dissolution of stannous oxide into Sn^{2+} as opposed to Ni^{2+} for transpassive dissolution in the passive oxide layer [28]. When considering the surface morphology (Fig. 2) and the weight loss curves of the Sn and Sn-Ni alloy (Fig. 3), it is clear that the existence of Ni in the alloy inhibits the dissolution of Sn species and helps the formation of passive oxide layers because nickel is easily passivated[39]. Evidently, the stable passive oxide layer composed of $Ni(OH)_2$, SnO and SnO_2 that forms on the surface of the Sn-Ni alloy is responsible for the excellent anti-corrosion properties of the Sn-Ni alloy in a chloride-containing neutral medium.

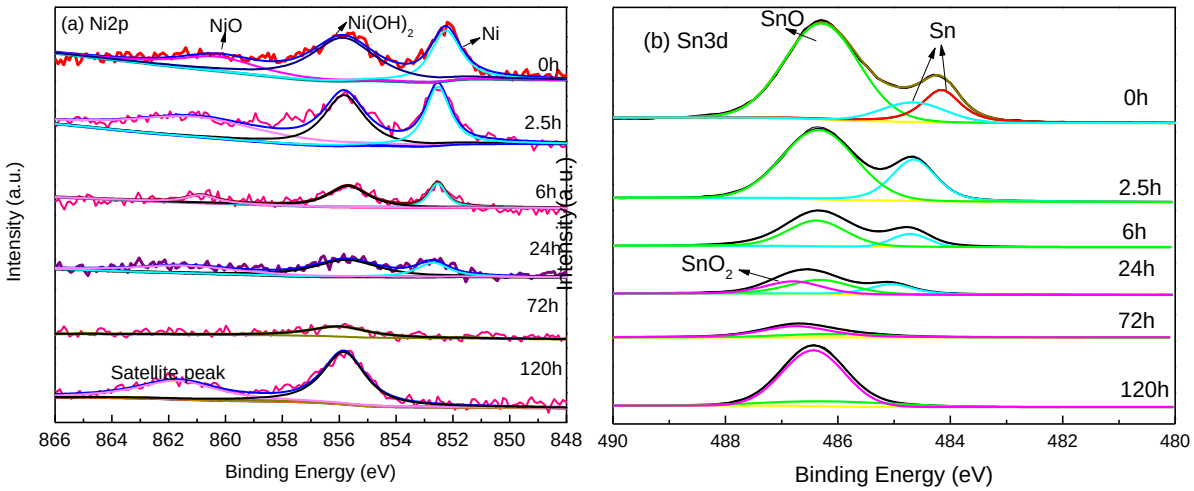

Figure 4. XPS spectra of $Ni2p_{3/2}$ (a) and $Sn3d_{5/2}$ (b) of the Sn-Ni alloy coating exposed to salt spray testing for different times

Table 1. The proportions of each peak after peak-fitting and atomic ratios under different conditions

Phase	0 h (%)	2.5 h (%)	6 h (%)	24 h (%)	72 h (%)	120 h (%)
NiO	21.9	28.9	23.1	25.4	-	-
$Ni(OH)_2$	49.3	30.4	50.5	47	100	100
Ni	28.8	40.7	26.4	27.6	-	-
SnO_2	0	0	0	32.2	72. 1	84.0
SnO	71.3	70.4	75.0	42.5	27.9	16.0
Sn	28.7	29.6	25.0	25.3	-	-
Sn/Ni	2.7	2.2	1.4	1.2	1	1.2

EIS can be used to detect a change in the property of the oxide passivation film with different salt spray testing times. The electrochemical impedance spectra of the Sn-Ni alloy coating for different salt spray test times at the OCP in the 5% NaCl solution are shown in Fig. 5. All Nyquist diagrams show a semicircular arc in the relatively high frequency range. The capacitive loop indicates that the corrosion process of the Sn-Ni alloy coating is controlled by the charge transfer process [28, 40]. The charge transfer resistance (R_{ct}) can be easily estimated on the real impedance axis by extrapolating the impedance trend at the lowest frequencies, and this value corresponds to the extent of the anti-corrosive nature of the coatings [38, 41]. The protective properties of the film that forms on the surface of the Sn-Ni alloy increase with increasing diameter of the semicircle [42]. Before salt spray testing, the R_{ct} value of the Sn-Ni alloy coating is approximately 57200 Ω cm^2. After treatment with a salt spray, the R_{ct} values change to approximately 23000, 20900, 9700, 54200 and 55200 Ω cm^2 when the

testing time extends to 2.5 h, 6 h, 24 h, 72 h and 120 h, respectively. Evidently, the protective properties of the "natural" oxide film that formed upon air exposure are deteriorated due to erosion from the NaCl solution during the first 24 salt spraying and then recover when the surface of the alloy coating is eroded further. After 72 h of salt spraying, the surface is covered by a new compact oxide film composed of $Ni(OH)_2$, SnO and SnO_2. Hence, the excellent corrosion resistance of the Sn-Ni alloy in the NaCl solution is due to the regeneration of the compact passive film consisting of metallic oxides.

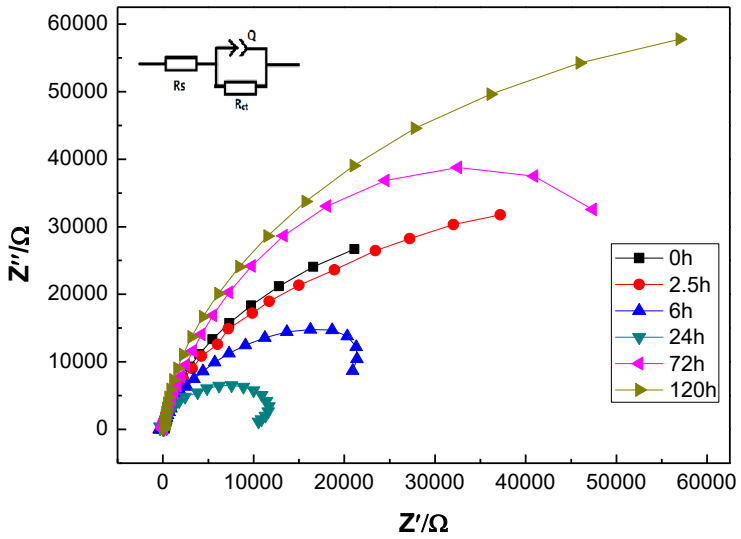

Figure 5. Nyquist plots of Sn-Ni alloy samples after salt spray testing for different times

A potential polarization test can be applied to evaluate the properties of the electrochemical corrosion resistance of the passive film that forms on the surface of the Sn-Ni alloy coating. Resistance to electrochemical corrosion can be estimated from the self-corrosive potential (E_{corr}) and the self-corrosive current (i_{corr}) calculated from E versus log(i). A high E_{corr} indicates a good resistance to electrochemical corrosion, and a low i_{corr} indicates a low corrosion rate[40, 43]. The recorded potentiodynamic polarization curves for the Sn-Ni coatings that are treated with different salt spray testing times in a 5% NaCl solution are presented in Fig. 6, and the parameters derived from the E versus log(i) plot are given in Table 2. The E_{corr} for the passive film on the Sn-Ni alloy coating shifts toward a slightly more negative value after 24 h of salt spraying, and the i_{corr} increases from 2.75 uA cm^{-2} to 7.23 uA cm^{-2}, indicating that the passive film that forms on the surface of the Sn-Ni alloy coating is destroyed due to erosion by the NaCl solution during the initial salt spraying stage. After 72 h of salt spraying, the E_{corr} and i_{corr} of the passive film on the Sn-Ni alloy coating return to their original states before the salt spray testing, revealing that the oxide film that forms during exposure to the NaCl solution has a high resistance to electrochemical corrosion. The change in i_{corr} is related to the change in the R_{ct} value of the passive film that forms on the surface of the Sn-Ni alloy at different salt spraying times. The larger the R_{ct} value is, the lower the corrosion current. Compared to that of the fresh Sn-Ni alloy, the regeneration of the electrochemical anti-corrosion layer on the Sn-Ni alloy in an erosive medium indicates the self-repairing ability of the oxide passive film on the surface of the Sn-Ni alloy.

Without nickel, the Sn erosion occurs continuously during salt spraying because tin is not passivated like nickel. The formation of the stable passivation film on the surface of a Sn-Ni alloy should correspond to the self-repairing ability of a Sn-Ni alloy against electrochemical corrosion.

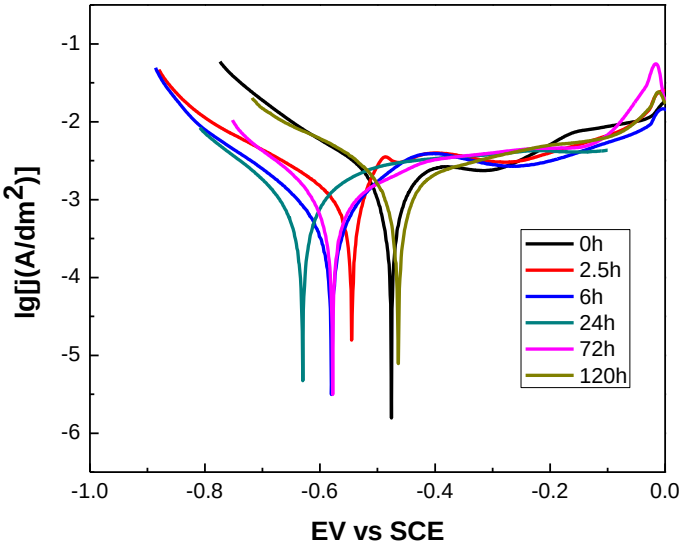

Figure 6. Polarization curves for Sn-Ni alloy in 5 wt.% NaCl solution for different salt spray testing times

Table 2. Corrosion parameters obtained from polarization studies for Sn-Ni coatings in 5 wt. % NaCl solution for different salt spray testing times

	0 h	**2.5 h**	**6 h**	**24 h**	**72 h**	**120 h**
E_{corr} (V)	-0.476	-0.544	-0.581	-0.630	-0.574	-0.463
I_{corr} (uA/cm^2)	2.75	4.85	6.35	7.23	3.80	2.47

A change in the surface composition during the spraying test may affect the morphology of the Sn-Ni alloy surface. Fig. 7 shows SEM images of Sn-Ni alloy coatings exposed to a salt spray solution containing 5 wt. % NaCl for different time intervals. Before salt spray testing, the Sn–Ni alloy deposit is compact, uniform and there are no distinguishable boundaries between grains (Fig. 7a). After exposure to the salt spray, the grain boundaries become clear during the first 24 h of exposure (Fig. 7 b, c and d) and then become unclear and blurry again (Fig. 7 e and f). After 120 h of salt spray testing, the surface of the Sn-Ni alloy coating is still compact, and the porosity of the Sn–Ni layer is nearly negligible, although the gloss on the Sn-Ni alloys coating somewhat decreases. Although a change in the morphology of the Sn-Ni alloy coating with the exposure time to salt spray indicates that the Sn-Ni alloy corrodes to some extent, the passivation film that forms can exist on the surface of the alloy in the corroded system (Fig. 5) and remains compact, which hinders the further erosion of the alloy and maintains the properties of the Sn-Ni alloy.

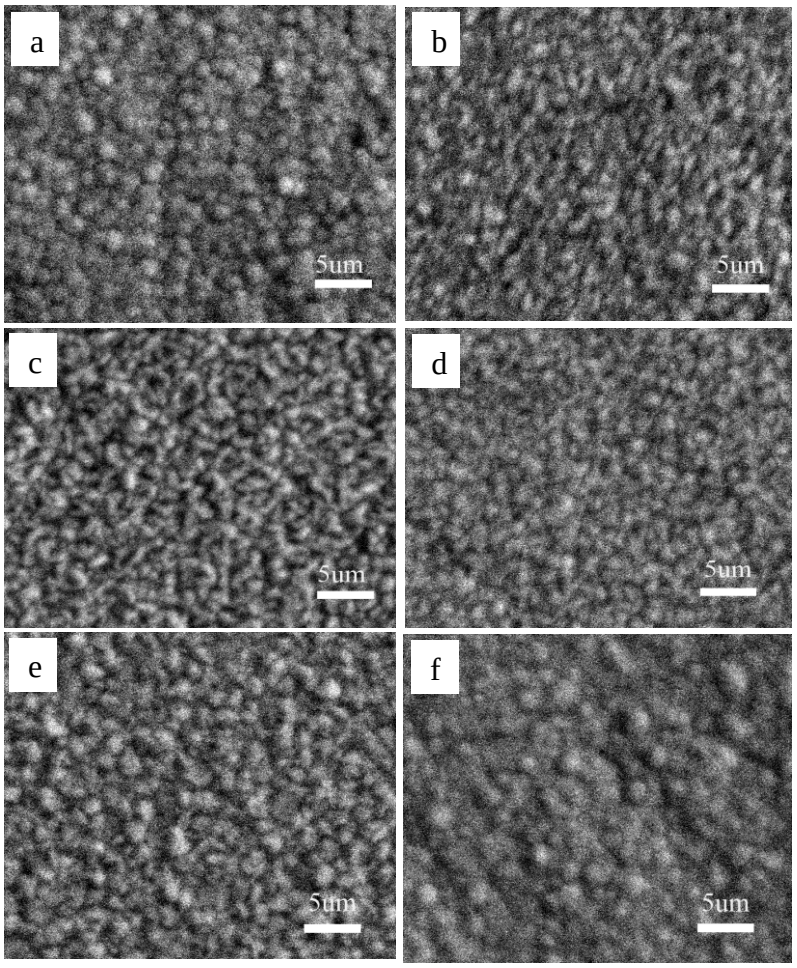

Figure 7. SEM images of Sn-Ni alloy exposed to salt spray for (a) 0 h, (b) 2.5 h, (c) 6 h, (d) 24 h, (e) 72 h and (f) 120 h.

The XRD patterns of the Sn-Ni alloy coatings exposed to the salt spray testing for different times are shown in Fig. 8. Before 72 h of salt spray testing, even though no evident phase change is detected at the surface of the Sn-Ni alloy coatings, but the intensity of the peaks at 43.3° and 50.6° changes. This suggests that the quantitative ratio of the Ni and Ni_3Sn phases changes. When the salt spray testing time is extended to 120 h, several small peaks appear in addition to the peaks of the Sn-Ni alloy itself, indicating that some chemical reactions evidently take place on the surface of Sn-Ni alloy and produce new phases when the alloy experiences a sufficient amount of salt spray testing. Considering the possible reactions, the new peaks located at 30.6°, 33.5°, 44.2°, 50.5° and 55.6° may result from the regeneration of the SnO (JCPDS07-0195 and JCPDS 24-1342) and $Ni(OH)_2$ phases (JCPDS02-1112). The presence of new phases indicates that the surface of the Sn-Ni alloy changes, a new oxide film forms when Sn-Ni is exposed to a salt spray, and corrosion reactions occur. According to the XPS results (Fig. 4), there is an oxide film that forms in the air on the surface of the deposited Sn-Ni alloy. Here, the absence of these oxide materials in the XRD spectra for the sample treated for less than 72 h indicates that this oxide film is very thin. Compared to that for the surface of Sn-Ni alloy treated in salt spray for 72 h, the presence of new peaks in the XRD spectrum of the Sn-Ni alloy

coating after 120 h salt spray testing indicates that the amount of the oxide film increases as the salt spray testing time increases. The increased oxides are composed of an apparent oxide passivation film that is compact and improves the anti-corrosion ability of the Sn-Ni alloy.

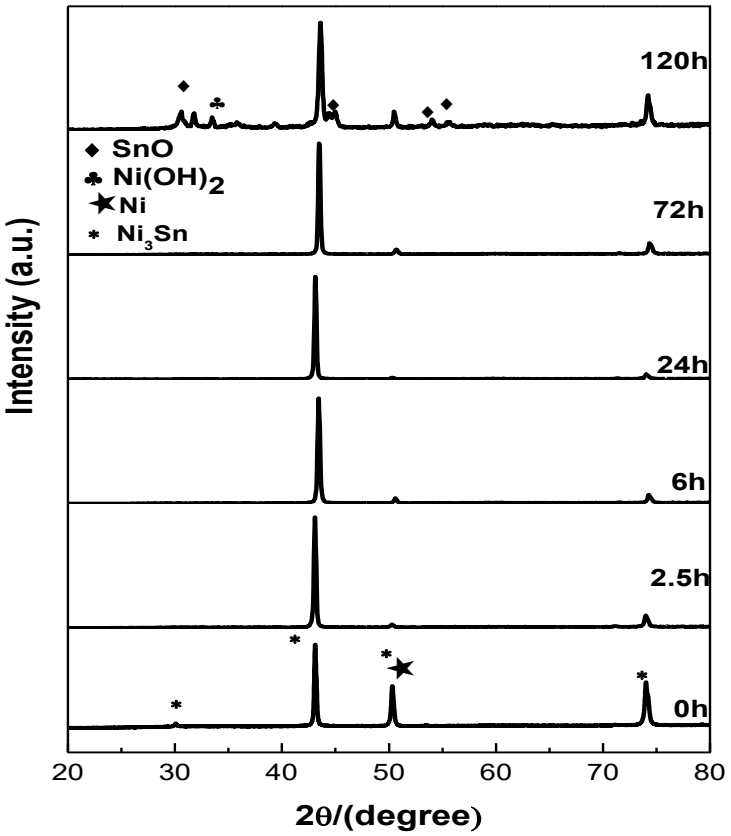

Figure 8. X-ray spectra of Sn-Ni alloy coatings for different periods of salt spray testing in 5 wt. % NaCl solution.

4. CONCLUSIONS

A Sn-Ni alloy containing approximately 33 wt. % Ni was electrodeposited from a pyrophosphate electrolyte, and its corrosion behavior was studied by a neutral salt spray method that used a 5 wt. % NaCl solution and electrochemical methods. Compared to that for the pure Sn coating, the Sn-Ni alloy shows a high corrosion resistance in neutral solution. The physical measurements indicate that there is a thin compact passive film on the surface of the as-deposited Sn-Ni alloy coating. At the initial stage of salt spray testing, the passive film that formed in the air on the surface of the Sn-Ni alloy is destroyed by the medium containing NaCl, and the metallic Sn and Ni in the Sn-Ni alloy are dissolved to form their oxides. The newly formed oxides produce a new passive film that covers the surface of Sn-Ni alloy and provides excellent resistance to electrochemical corrosion. The good corrosion resistance of the Sn–Ni alloy is due to the regeneration of a passive film composed of nickel and tin oxides. The good anti-corrosion performance of the Sn–Ni alloy suggests that it can be used for applications in neutral mediums containing NaCl.

ACKNOWLEDGEMENT
This study was funded by authors themselves. The authors declare that they have no conflict of interest.

References

1. S.C. Britton and R.M. Angles, *J. Electrodep. Tech. Soc.*, 27 (1951) 293.
2. G. Ghosh, *Metall. Mater. Trans. A.*, 30(1999) 1481.
3. C. Schmetterer, H. Flandorfer, K.W. Richter, U. Saeed, M. Kauffman, P. Roussel and H. Ipser, *Intermetallics*, 15(2007) 869.
4. R.Y. Tian, C.J. Hang, Y.H. Tian and J.Y. Feng, *J. Alloys Compd.,* 777(2019) 463
5. S.K. Jalota, *Met. Finish.,* 99(2001) 320.
6. K. Ulman, S. Maroufi, S. Bhattacharyya and V. Sahajwalla, *J. Clean Prod.*, 198(2018) 1485.
7. C. Langer, W. Wendland, K. Honold, L. Schmidt, J.S. Gutmann and M. Dornbusch, *Eng. Fail. Anal.*, 91(2018) 255.
8. R. Schneider, C. Cavalin, M. Barros and C. Tavares, *Chem. Eng. J.*, 132(2007) 355.
9. J.L. Ovesen, Y.X. Fan, J. Chen, M. Medvedovic, Y. Xia and A. Puga, *Toxicology*, 316(2014) 14.
10. 10 T. Kobayashi, H. Kanematsu, M. Yoshitake and T. Oki, *Trans. Inst. Met. Finish.*, 80(2002) 194.
11. B. Subramanian, S. Mohan and S. Jayakrishnan, *J. Appl. Electrochem.*, 37(2007) 219.
12. Q.G. Han, D. Geng, Z.W. Han, F.X. Wang, X. Li, Y.S. Deng, J.Q. Zhang, S.C. Niu and Y.N. Mu, *J. Electroanal. Chem.*, 822(2018) 17.
13. X.H. Chang, Z.L. Liu, B.X. Sun, Z.W. Xie, J. Zheng and X.G. Li, *Electrochim. Acta*, 267(2018) 1.
14. X.G. Liu, X.L. Li, J.Y. Yu and Y.P. Sun, *Mater. Lett.*, 223(2018) 203.
15. L. Huang, H.B. Wei, F.S. Ke, X.Y. Fan, J.T. Li and S.G. Sun, *Electrochim. Acta,* 54(2009) 2693.
16. X. Dong, W.B. Liu, X. Chen, J.Z. Yan, N. Li, S.Q. Shi, S.C. Zhang and X.S. Yang, *Chem. Eng. J.*, 350(2018) 791.
17. T.L. Nguyen, D.S. Kim, J. Hur, M.S. Park and II T. Kim, *Electrochim. Acta*, 278(2018) 25.
18. K. Zhuo, M.G. Jeong, M.S. Shin, W.W. Chun, J.W. Bae, P.J. Yoo and C.H. Chung, *Appl. Surf. Sci.*, 322(2014) 15.
19. B.M. Jovic, U.C. Lacnjevac, N.V. Krstajic and V.D. Jovic, *Electrochim. Acta*, 114(2013) 813.
20. J.W. Cuthbertson, N. Parkinson and H.P. Rooksby. *J. Electrochem. Soc.*, 100(1953) 107.
21. E. Rudnik. *Key Eng. Mater.*, 641(2015) 149.
22. U. Lacnjevac. B.M. Jovic and V.D. Jovic, *J. Electrochem. Soc.*, 159(2012) D310.
23. E. Rudnik. *J. Electroanal. Chem.*, 726(2014) 97.
24. M. Clarke and R.G. Elbourne, *Electrochim. Acta*, 16(1971) 1949.
25. T.P. Hoar, M. Talerman and E. Trad, *Nat. Phys. Sci.*, 244(1973) 41.
26. S.A.M. Refaey, F. Taha and T.H.A. Hasanin, *Appl. Surf. Sci.*, 227 (2004) 416.
27. A.P.I. Popoola, C.A. Loto, C.O. Osifuye, V.S. Aigbodion and O.M. Popoola, *Alexandria Eng. J.*, 55(2016) 2901.
28. S.A.M. Refaey, F. Taha and T.H.A. Hasanin, *Electrochim. Acta*, 51(2006) 2942.
29. Z.B. Bao, Q.M. Wang, W.Z. Li, J. Gong, T.Y. Xiong and C. Sun, *Corr. Sci.*, 50(2008) 847.
30. E.D. Kiosidou, A. Karantonis, G.N. Sakalis and D.I. Pantelis, *Corr. Sci.*, 137(2018) 127.
31. C. Schmetterer, H. Flandorfer and H. Ipser, *J. Alloys Compd.*, 486(2009) L8.
32. A. Zemanova, A. Kroupa and A. Dinsdale, *Monatsh Chem.*, 143(2012) 1255.
33. Y. Wang, L. Zhang, J.K. Xiao, W. Chen, C.F. Feng, X.P. Gan and K.C.Zhou, *Tribol. Int.*, 94(2016) 260.
34. J. F. Silvain and O. Fouassier, *Surf. Interface Anal.*, 36(2004) 769.
35. H.W. Neshitt, D. Legrand and G.M. Bancroft, *Phys. Chem. Miner.*, 27 (2000) 357.
36. N. Sato and G. Okamoto, *J. Electrochem. Soc.*, 110(1963) 605.

37. B. MacDougall，D.F. Mitchell and M.J. Graham, *J. Electrochem. Soc.*, 132(1985) 2553.
38. M. Pugh, L.M. Warner and D. R. Gabe, *Corr. Sci.*, 7(1967) 807.
39. Y.K. Kang and W.K. Paik, *Surf. Sci.*, 182 (1987) 257.
40. L. Anicai, A. Petica, S. Costovici, P. Prioteasa and T. Visan, *Electrochim. Acta* , 114(2013) 868.
41. R. Berlia, M.K. Punith Kumar and C. Srivastava, *RSC Adv.*, 5(2015) 71413.
42. R. Sekar, C. Eagammai and S. Jayakrishnan, *J. Appl. Electrochem.*, 40(2010) 49.
43. L.Y. Cui, G.B. Wei, R.C. Zeng, S.Q. Li, Y. H. Zou and E. H. Han, *Bioactive Mater.*, 3(2018) 245.